Electronic Supplementary Material (ESI) for Dalton Transactions.

Supporting information

An enhanced photoreduction efficiency of Cr(VI) driven by visible light in a new Zr-based metal-organic framework modified by hydroxyl groups

Duc T. Nguyen,[a] Khang M. V. Nguyen,[a] Huy K. Duong,[a] Binh T. Nguyen,[a] Mai D. K. Nguyen,[a] Dang B. Tran,[a] Quang-Hieu Tran,[b] Tan L. H. Doan[c,d] and My V. Nguyen*[a]

[a] Faculty of Chemistry, Ho Chi Minh City University of Education, Ho Chi Minh City, 700000, Vietnam.

[b] Basic Sciences Department-Saigon Technology University, Ho Chi Minh City 700000, Vietnam, 180 Cao Lo, Ward 4, District 8, Ho Chi Minh City, Vietnam.

[c] Center for Innovative Materials and Architectures (INOMAR), Ho Chi Minh City, Vietnam.

[d] Vietnam National University, Ho Chi Minh City, Vietnam.

*To whom correspondence should be addressed: mynv@hcmue.edu.vn

Section S1. Nuclear Magnetic Resonance (NMR) Spectroscopy

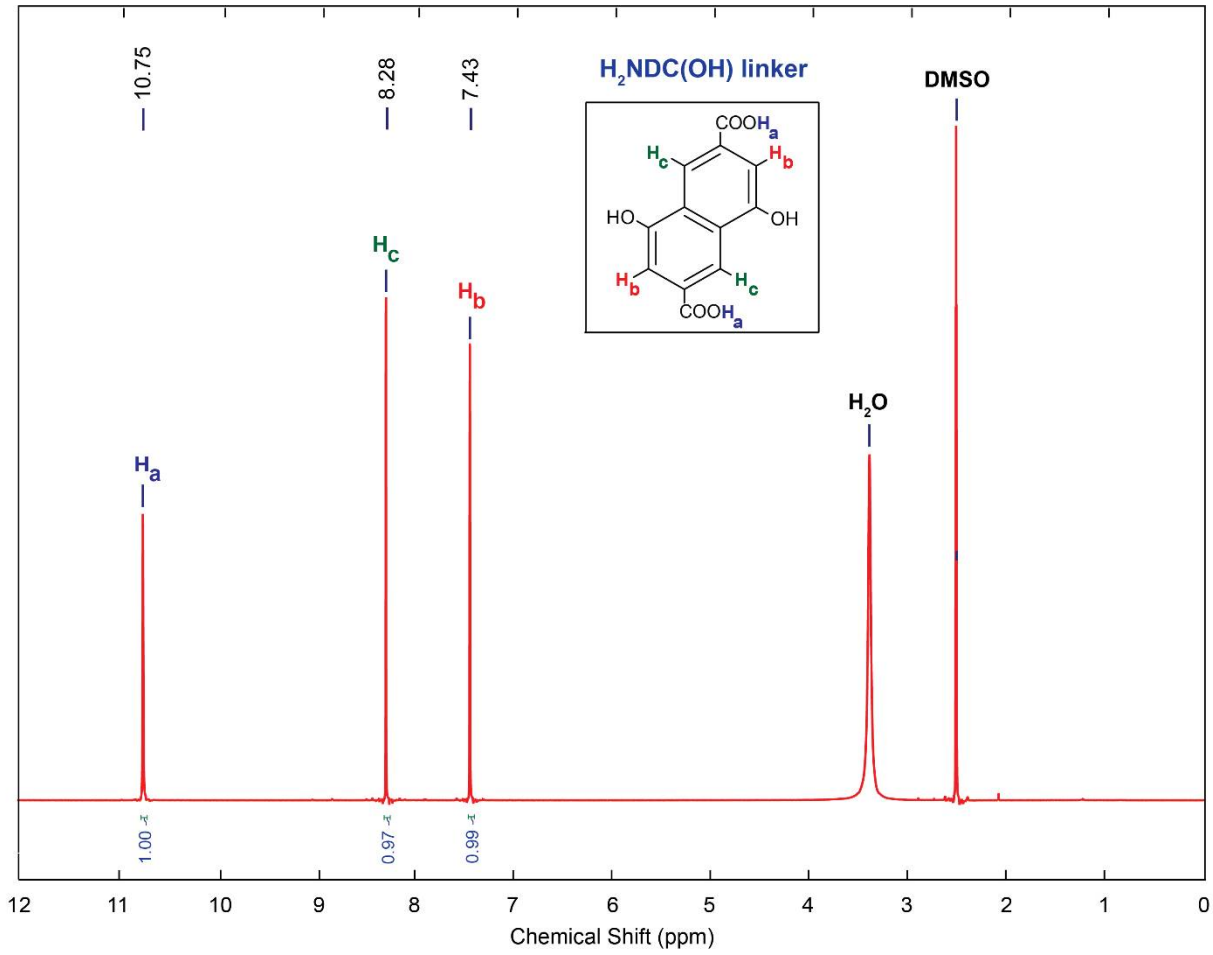

Figure S1. ^{1}H-NMR spectrum of H_2NDC(OH) linker in DMSO solvent.

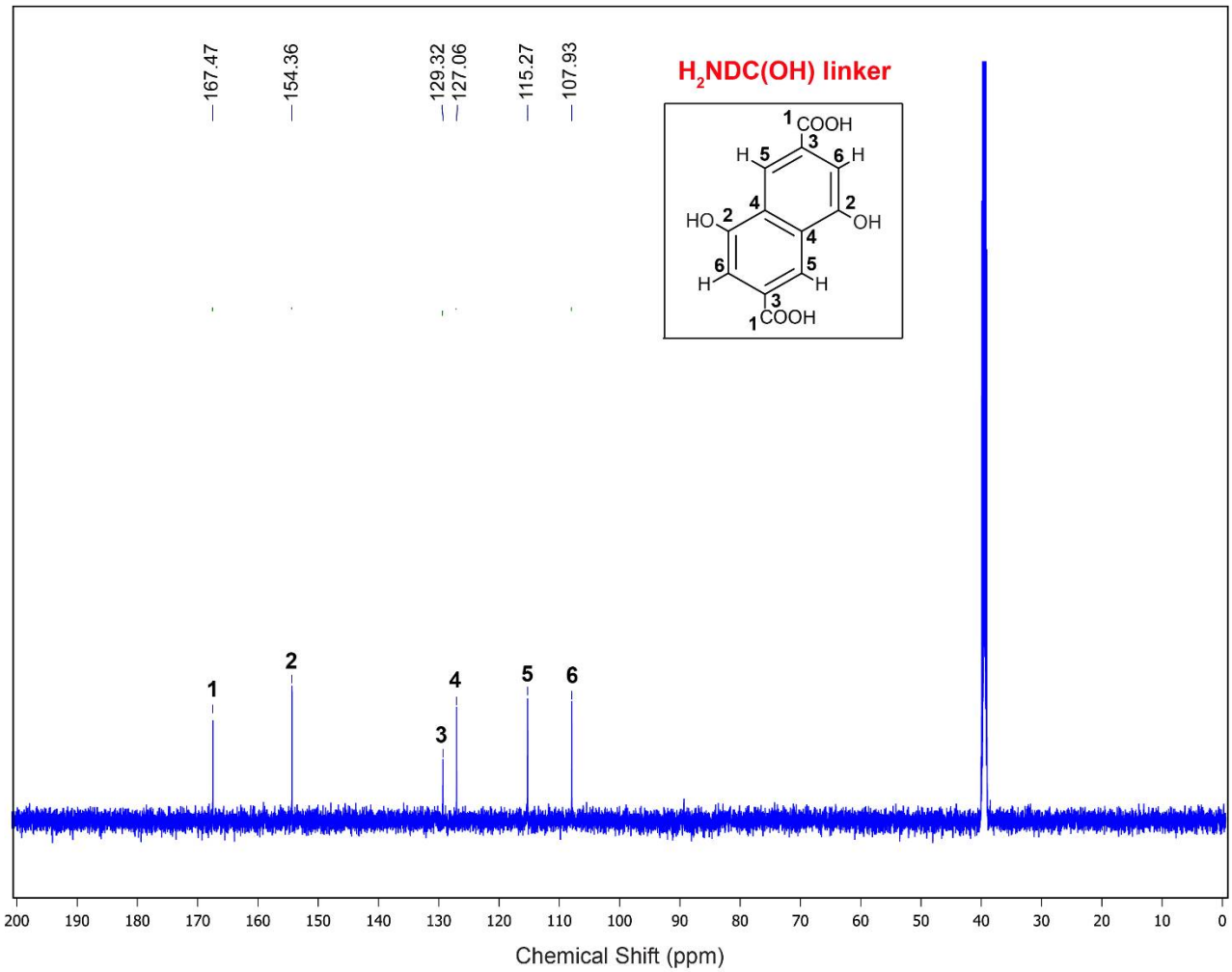

Figure S2. ^{13}C-NMR spectrum of H_2NDC(OH) linker in DMSO solvent.

Section S2. The standard curve of Cr(VI)

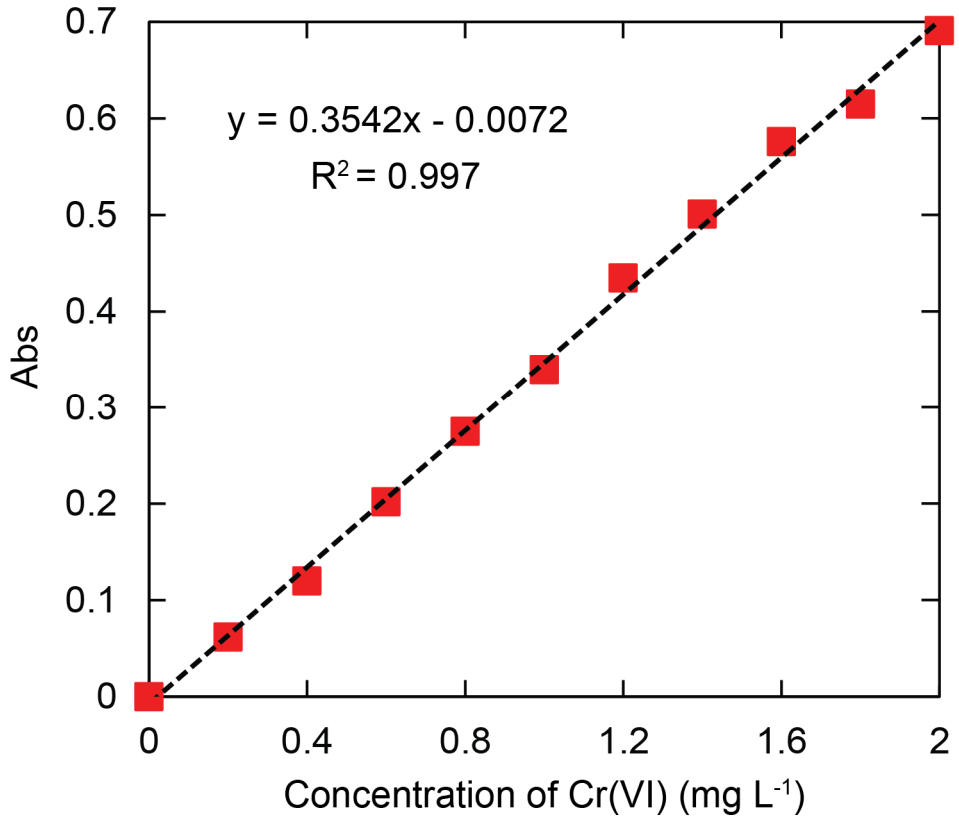

Figure S3. The relationship between the absorbed intensity of the Cr(VI) complex via the DPC method and the Cr(VI) different concentrations of 0 – 2 mg L^{-1} by linear fitting.

Section S3. Raman Spectroscopy

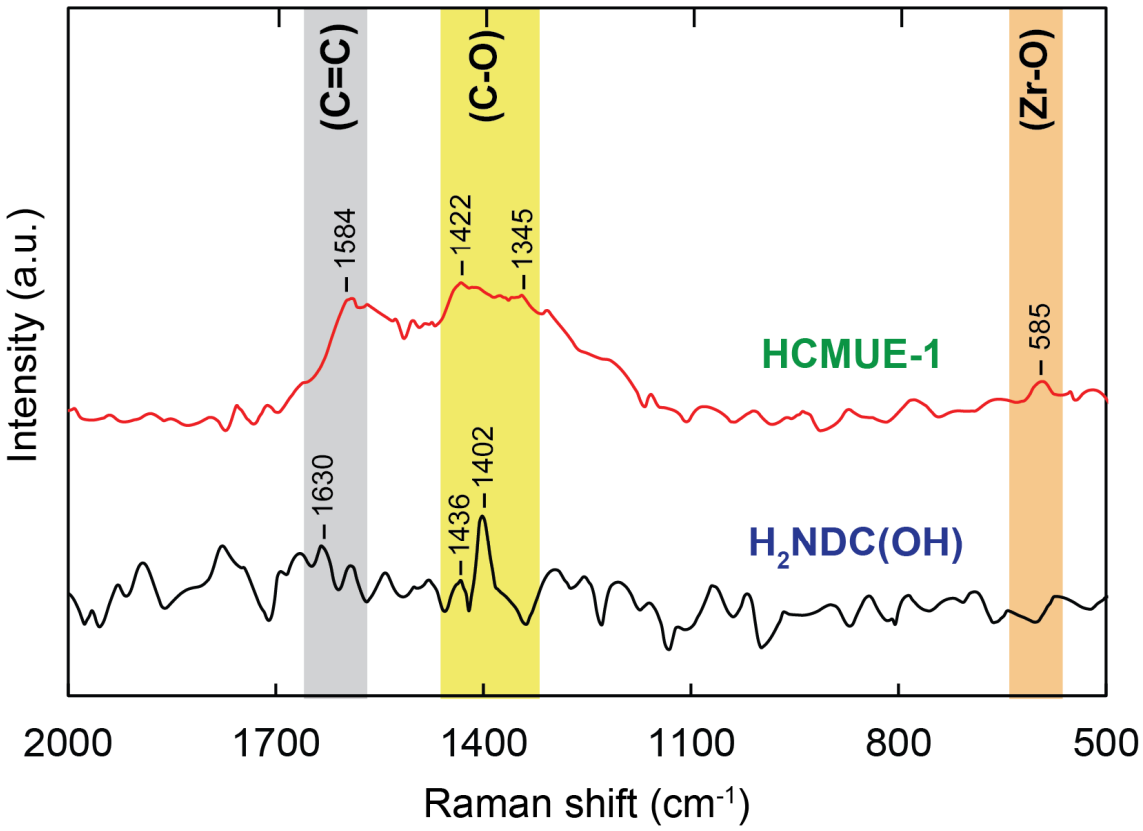

Figure S4. Raman spectrum of activated HCMUE-1 (red) in comparison with $H_2NDC(OH)$ linker (black).

Section S4. N_2 isotherm adsorption analysis at 77K

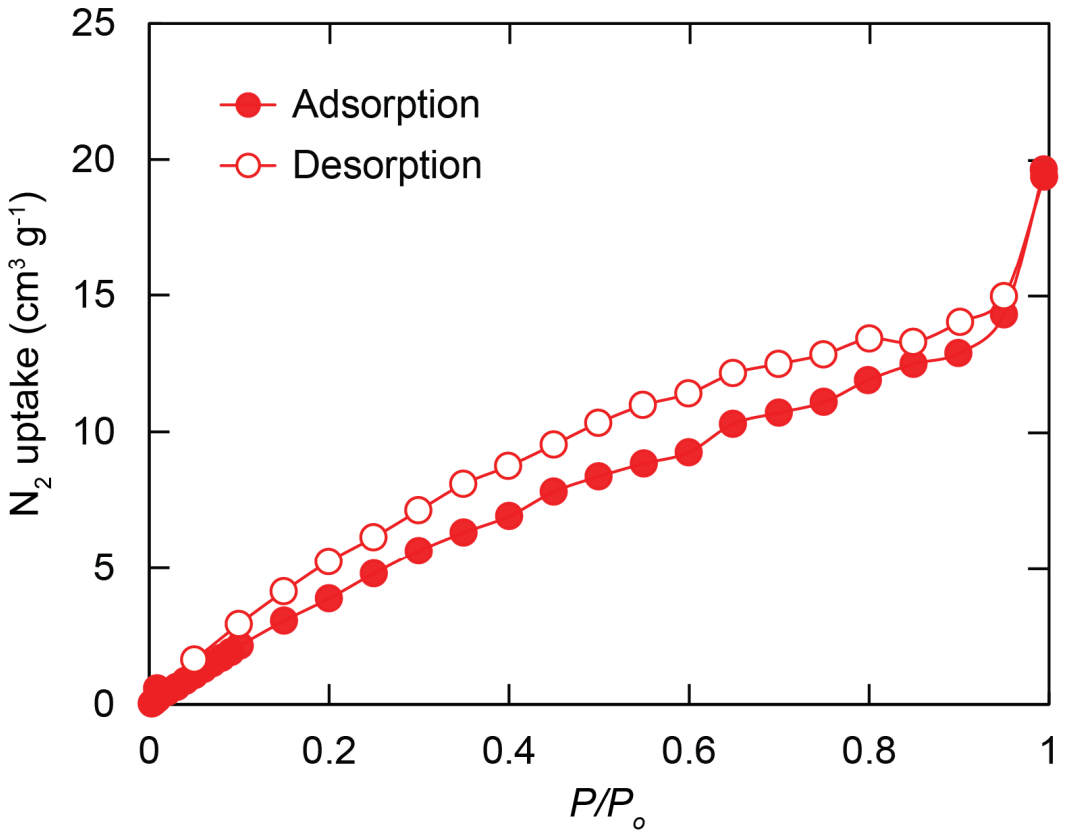

Figure S5. N_2 isotherm curve of HCMUE-1 material at 77K. The closed and open circles symbolize the adsorption and desorption branches of the isotherm, respectively.

Section S5. XPS Spectroscopy

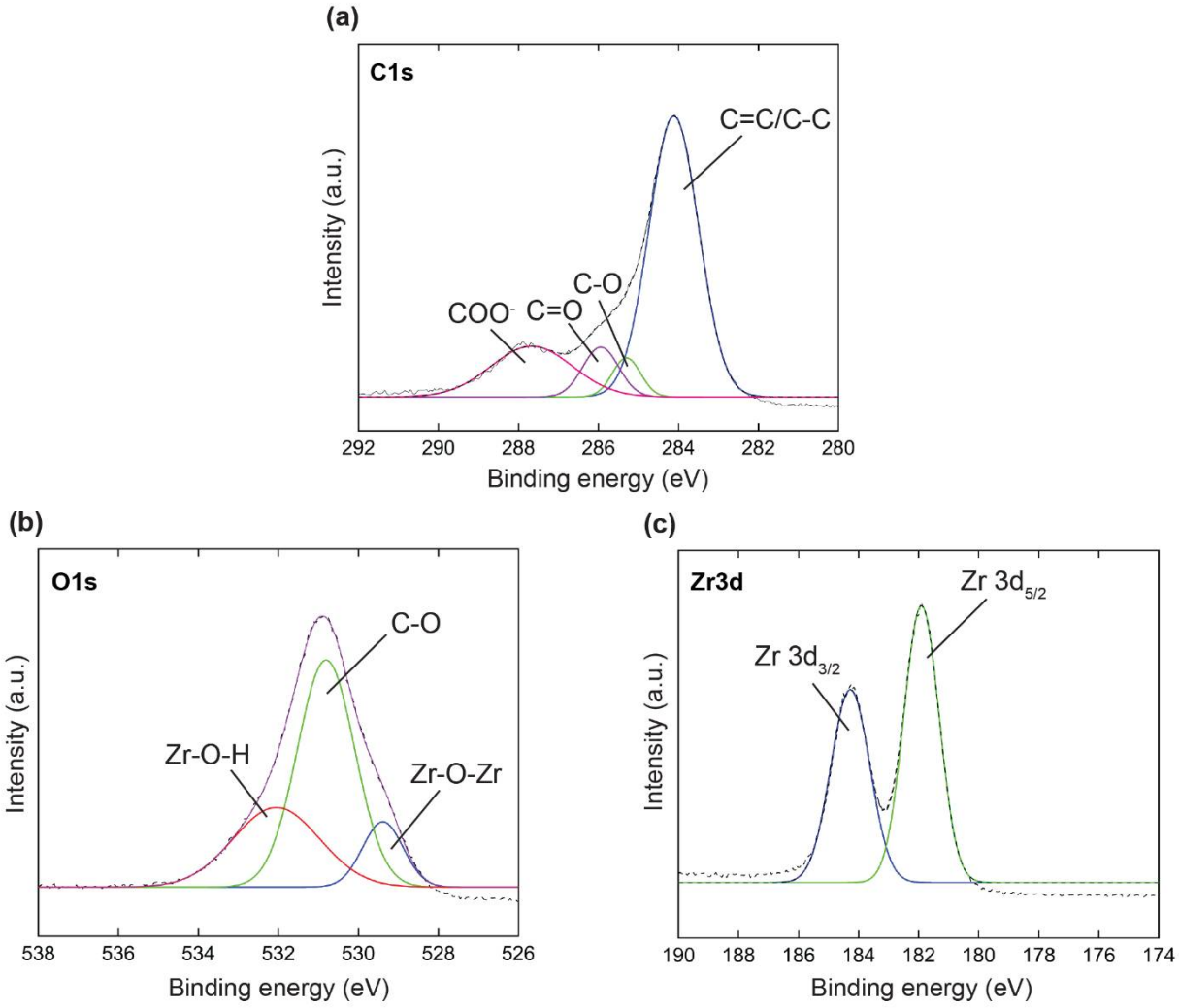

Figure S6. The XPS analysis of HCMUE-1 after photocatalysis: high-resolution spectrum of C 1s in HCMUE-1 (a); high-resolution spectrum of O 1s in HCMUE-1 (b); high-resolution spectrum of Zr 3d in HCMUE-1 (c).

Section S6. Photoluminescence spectra and time-resolved fluorescence analysis

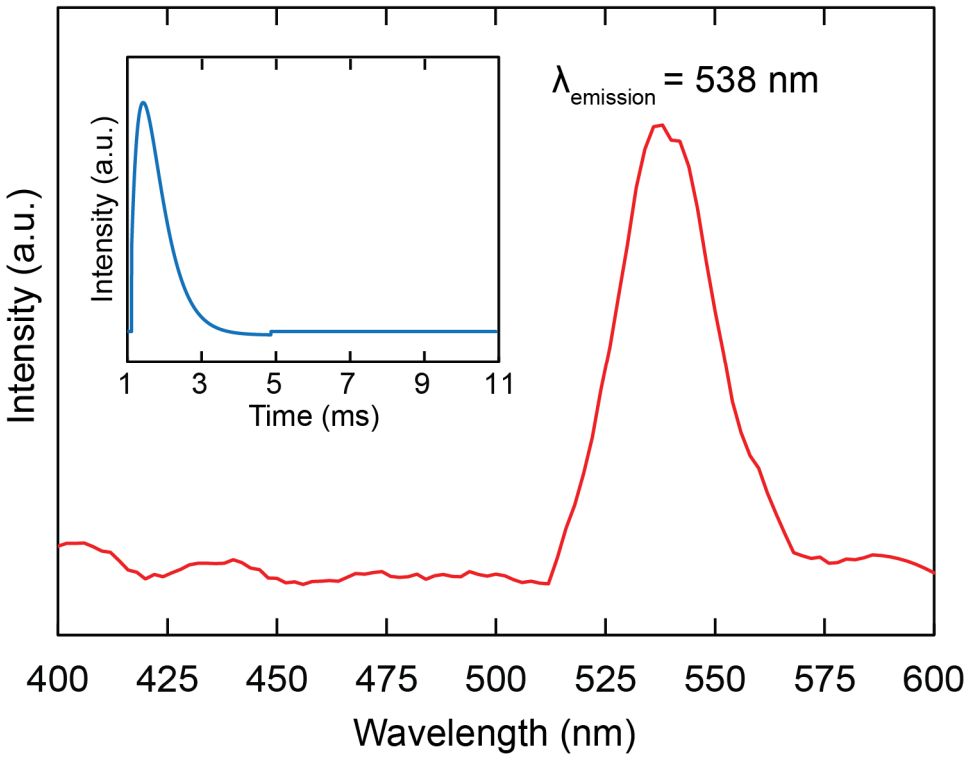

Figure S7. Photoluminescence spectra and time-resolved fluorescence decay traces (inset) were collected for HCMUE-1 material with an excitation wavelength of 270 nm.

Section S7. Photocatalyic kinetic model for the Cr(VI) reduction

Photoreduction kinetic. The pseudo-first-order kinetic are utilized to determine the photoreduction rate of Cr(VI), which is displayed by the eqn:

$$\ln\left(\frac{C_t}{C_o}\right) = -k_1 t$$

Where C_t and C_o are the Cr(VI) concentration at t and original time, k_1 are the rate constant of pseudo-first-order**.**

Table S1. The Cr(VI) photoreduction efficiency of HCMUE-1 in comparison with other previously reported materials

Material	Dosage of catalyst ($g\ L^{-1}$)	Initial concentration ($mg\ L^{-1}$)	Light source	Overall degradation efficiency (%)	Time (min)	Ref.
$SrTiO_3$	1.0	4.8	Visible light	99	240	[1]
Fe-g-C_3N_4/MoS_2	0.6	9.6	Visible light	91.4	150	[2]
OH-TiO_2	1.0	10	Visible light	88	30	[3]
Ag-BiOCl	1.0	10	Visible light	86	180	[4]
NNU-36	0.375	10	Visible light	95.3	60	[5]
MIL-53(Fe)	1.0	20	Visible light	66	40	[6]
Ag/AgCl@MIL-53(Fe)	0.4	10	Visible light	99.4	240	[7]
Pt@MIL-100(Fe)	1.0	20	Visible light	100	8	[8]
MIL-68(In)-NH_2	1.0	20	Visible light	97	80	[9]
g-C_3N_4/UiO-66	0.5	10	White light	99	40	[10]
UiO-66-NH_2(Zr)	0.5	5	Sunlight	98	120	[11]
UiO-66$(OH)_2$	0.2	8	Visible light	100	10	[12]
RGO-UiO-66(NH_2)	0.5	10	Visible light	100	100	[13]
MIL-53-NH_2	0.5	8	Visible light	15	60	[14]
MIL-53/WO_3	1.0	45	Sun light	94	240	[15]
MIL-101-NH_2/g-C_3N_4	1.0	20	Sun light	66	90	[16]
MIL-100/$Bi_{12}O_{17}C_{12}$	0.5	10	Visible light	99.2	120	[17]
DUT-52	0.2	20	Visible light	30	120	This study
HCMUE-1	**0.2**	**10**	**Visible light**	**100**	**30**	
	0.2	**20**	**Visible light**	**98**	**90**	
	0.2	**20**	**Visible light**	**100**	**120**	

References

[1] D. Yang, Y. Sun, Z. Tong, Y. Nan and Z. Jiang, Fabrication of bimodal-pore $SrTiO_3$ microspheres with excellent photocatalytic performance for Cr(VI) reduction under simulated sunlight, *J. Hazard. Mater.*, 2016, **312**, 45-54.

[2] X. Wang, M. Hong, F. Zhang, Z. Zhuang and Y. Yu, Recyclable nanoscale zero valent iron doped g-C_3N_4/MoS_2 for efficient photocatalysis of RhB and Cr(VI) driven by visible light, *ACS Sustain. Chem. Eng.*, 2016, **4**, 4055-4063.

[3] Y. Li, Y. Bian, H. Qin, Y. Zhang and Z. Bian, Photocatalytic reduction behavior of hexavalent chromium on hydroxyl modified titanium dioxide, *Appl. catal. B: environ.*, 2017, **206**, 293-299.

[4] H. Li and L. Zhang, Oxygen vacancy induced selective silver deposition on the {001} facets of BiOCl single-crystalline nanosheets for enhanced Cr(VI) and sodium pentachlorophenate removal under visible light, *Nanoscale*, 2014, **6**, 7805-7810.

[5] H. Zhao, Q. Xia, H. Xing, D. Chen and H. Wang, Construction of pillared-layer MOF as efficient visible-light photocatalysts for aqueous Cr(VI) reduction and dye degradation, *ACS Sustain. Chem. Eng.*, 2017, **5**, 4449-4456.

[6] R. Liang, F. Jing, L. Shen, N. Qin and L. Wu, MIL-53(Fe) as a highly efficient bifunctional photocatalyst for the simultaneous reduction of Cr(VI) and oxidation of dyes, *J. Hazard. Mater.*, 2015, 287, 364-372.

[7] Q. Liu, C. Zeng, L. Ai, Z. Hao and J. Jiang, Boosting visible light photoreactivity of photoactive metal-organic framework: Designed plasmonic Z-scheme Ag/AgCl@MIL-53-Fe, *Appl. Catal. B: Environ.*, 2018, **224**, 38-45.

[8] R. Liang, F. Jing, L. Shen, N. Qin and L. Wu, M@MIL-100(Fe) (M = Au, Pd, Pt) nanocomposites fabricated by a facile photodeposition process: Efficient visible-light photocatalysts for redox reactions in water, *Nano Res.*, 2015, **8**, 3237-3249.

[9] R. Liang, R. Huang, X. Wang, S. Ying, G. Yan and L. Wu, Functionalized MIL-68(In) for the photocatalytic treatment of Cr(VI)-containing simulation wastewater: Electronic effects of ligand substitution, *Appl. Surf. Sci.*, 2019, **464**, 396-403.

[10] X.-H. Yi, S.-Q. Ma, X.-D. Du, C. Zhao, H. Fu, P. Wang and C.-C. Wang, The facile fabrication of 2D/3D Z-scheme g-C3N4/UiO-66 heterojunction with enhanced photocatalytic Cr(VI) reduction performance under white light, *Chem. Eng. J.*, 2019, **375**, 121944.

[11] X. -D. Du, X. -H. Yi, P. Wang, W. Zheng, J. Deng and C. -C. Wang, Robust photocatalytic reduction of Cr(VI) on UiO-66-NH_2(Zr/Hf) metalorganic framework membrane under sunlight

irradiation, *Chem. Eng. J.*, 2019, **356**, 393-399.

[12] H. Xie, D. Ma, W. Liu, Q. Chen, Y. Zhang, J. Huang, H. Zhang, Z. Jin, T. Luo and F. Peng, Zr-based MOFs as a new photocatalysts for rapid reduction of Cr(VI) in water, *New J. Chem.*, 2020, **44**, 7218-7225.

[13] L. Shen, L. Huang, S. Liang, R. Liang, N. Qin and L. Wu, Electrostatically derived self-assembly of NH_2-mediated zirconium MOFs with graphene for photocatalytic reduction of Cr(VI), *RSC Adv.*, 2014, **4**, 2546-2549.

[14] L. Shi, T. Wang, H. Zhang, K. Chang, X. Meng, H. Liu and J. Ye, An amine-functionalized iron(III) metal-organic framework as efficient visible-light photocatalyst for Cr(VI) reduction, *Adv. Sci.*, 2015, **2**, 1500006.

[15] A. A. Oladipo, MIL-53(Fe)-based photo-sensitive composite for degradation of organochlorinated herbicide and enhanced reduction of Cr(VI), *Process Saf. Environ. Prot.*, 2018, **116**, 413-423.

[16] D. Pattappan, K. V. Kavya, S. Vargheese, R. T. R. Kumar and Y. Haldorai, Graphitic carbon nitride/NH_2-MIL-101(Fe) composite for environmental remediation: visible-light-assisted photocatalytic degradation of acetaminophen and reduction of hexavalent chromium, *Chemosphere*, 2022, **286**, 131875.

[17] Li, H.; Zhao, C.; Li, X.; Fu, H.; Wang, Z.; Wang, C. -C. Boosted photocatalytic Cr(VI) reduction over Z-scheme MIL-53(Fe)/$Bi_{12}O_{17}Cl_2$ composites under white light, *J. Alloy. Compd.*, 2020, **844**, 156147.